RSC Advances

PAPER

Check for updates

Aggregation prevention: reduction of graphene oxide in mixed medium of alkylphenol polyoxyethylene (7) ether and 2-methoxyethanol†

Heng Su,[a] Chaocan Zhang, [iD] *[a] Xi Li, [iD] [b] Lili Wu[a] and Yanjun Chen[a]

Graphene has attracted great interest due to its extensive applications in optoelectronic and electronic circuits and devices. However, reduction of graphene oxide (GO) to graphene is a process in which hydrophilic GO converts to hydrophobic graphene. Very little is known about the aggregation of graphene and the cause of performance degradation by general chemical reduction methods as the single reaction medium presents difficulty in satisfying the good dispersion of hydrophilic GO and hydrophobic graphene simultaneously. In this paper, we report a mixed medium of alkylphenol polyoxyethylene (7) ether (OP-7) and 2-methoxyethanol (EGM) for the preparation of graphene. The strong polar nature of EGM provides a good dispersion environment for GO, while the π–π interaction between the π-electrons in nonionic surfactant OP-7 aromatic ring structure and the π-electrons in graphene make the hydrophobic graphene well dispersed and prevent aggregation. Moreover, the reduction temperature is not high and the reduction time is short. The electrical conductivity of graphene without high-temperature treatment reached 14 000 S m^{-1}. We have found the potential reduction mechanism of graphene and fundamentally solved the problem of aggregation. Our findings make it possible to process graphene materials using low-cost mixed medium processing techniques, providing a valuable reference for the large-scale preparation of graphene.

Introduction

Graphene is a one-atom-thick planar sheet of sp^2-hybridized carbon atoms arranged hexagonally. Graphene has extraordinary electrical, thermal, mechanical and other properties due to its unique two-dimensional crystal structure,[1,2] and it has emerged as an attractive material in electronics, optoelectronics and capacitors.[3,4] Among its various properties, the distinctive electronic properties of graphene has great potential applications in high-electron-mobility transistors,[5] supercapacitors[6–8] and solar cells.[9,10] Up to now, several fabrication routes for the production of graphene have been established, such as mechanical exfoliation,[11–13] chemical reduction of graphene oxide solution,[14–17] epitaxial growth[18,19] and chemical vapor deposition.[20,21] The chemical reduction method plays an important role in the prospect of potential industrialization.

[a]*Department of Materials Science and Engineering, Wuhan University of Technology, Wuhan 430070, China. E-mail: polymers@whut.edu.cn; suhengwhut@163.com; poly_wl@whut.edu.cn; yanjunchen@whut.edu.cn; Fax: +86 878 63157; Tel: +86 878 63157*

[b]*Department of Chemical Engineering and Life Sciences, Wuhan University of Technology, Wuhan 430070, China. E-mail: chemlixi@whut.edu.cn*

The chemical reduction method involves oxidizing graphite to form GO, and then reducing GO. Preparation of GO is conducted by methods such as Hummers method,[22] Brodie method[23] and Staudenmaier method[24] and then, the reduction of GO (RGO) is realized by using hydrazine,[25] hydrohalic acid[26] and sodium borohydride[27] as reducing agents. Until now, hydrazine hydrate, the most widely used reducing agent, was used in aqueous medium as a reductant to reduce GO (RGO$_{H2O}$). Previous studies have reported that RGO shows a distinct sharp peak between the 23.0° and 24.9° region of the XRD spectrum,[27–32] indicating that they have an ordered layer structure, and the electrical conductivity at room temperature is generally between 200 and 7200 S m^{-1}.[25,29,33–36] The value of conductivity fluctuates greatly, but the reason for this has not been studied in literature. In our opinion, ideal single-layer graphene should not have a typical layered structure, so there should be no sharp peak in the XRD spectrum. The edge of the graphite sheet is preferentially oxidized during the graphite oxidation stage, resulting in the oxidation degree of GO being higher than that in the middle region.[37,38] Therefore, the edge portion of GO will be preferentially reduced to hydrophobic graphene structure, while the middle region will be reduced slowly. Finally, the structure of RGO is hydrophobic in the marginal area, while the intermediate area is hydrophilic and due to the interaction forces between hydrophobic regions, RGO tends to overlap and aggregate into a layered structure.

This shows that the reduction of GO to RGO is a process where hydrophilic GO gets converted to hydrophobic RGO. Not only polar but also non-polar single reaction medium presents difficulties in satisfying the requirements of good dispersion for RGO. Furthermore, preventing aggregation during the reduction phase is the key to preparing RGO with excellent performance.

In this study, we designed a mixed medium that can simultaneously satisfy the well-dispersed hydrophilic GO and also prevent superimposed aggregation during the reduction process: OP-7 and EGM were mixed and used as the reaction medium and hydrazine hydrate was used as the reducing agent to reduce GO ($RGO_{OP-7/EGM}$). The strong polar nature of EGM provided a good dispersion environment for GO, while the π–π interaction between the π-electrons in the OP-7 aromatic ring structure and the π-electrons in the RGO enabled the effective dispersion of hydrophobic graphene in the reaction medium and prevented superimposed aggregation. The reduction routes and aggregation prevention mechanism are shown in Fig. 1. As a result, the XRD spectrum of the as-prepared $RGO_{OP-7/EGM}$ shows a broad diffraction peak between the $22.0°$ and $26.9°$, indicating that there is no typical layered structure. Furthermore, the reduction temperature is not high and the reduction time is short. The electrical conductivity of graphene prepared without high-temperature treatment was 14 000 S m^{-1}.

Experimental section

Chemicals and materials

Natural crystalline flake graphite (NG) (99.85% purity, 325 mesh), sulfuric acid (H_2SO_4, 98%), phosphoric acid (H_3PO_4, $\geq$ 85%), hydrochloric acid (HCl, 36%), anhydrous ethanol ($\geq$99.7%), 2-methoxyethanol (EGM $\geq$99%), hydrazine hydrate ($N_2H_4 \cdot H_2O$, 85%), hydrogen peroxide (H_2O_2, 30%), potassium permanganate ($KMnO_4$) and barium chloride ($BaCl_2$) were purchased from Sinopharm Chemical Reagent Co., Ltd. Alkylphenol polyoxyethylene (7) ether (OP-7) was purchased from Wen Hua Chemical Reagent Factory. Pure water with a frequency of 50 Hz (KQ-50, Kunshan Ultrasonic Instruments Co.) was used in all experiments.

Synthesis and dispersion of GO

GO was synthesized from natural crystalline flake graphite (NG) by a modified Hummers method.[22] NG (1 g) and potassium permanganate (5 g) were added in a mixture of sulfuric acid (98%, 81 mL) and phosphoric acid ($\geq$85 wt%, 9 mL), producing a slight exothermic reaction, which increased the temperature to 30–40 °C. The reaction was then heated to 50 °C without subsequent aging and stirred for 12 h. The reaction was then cooled to room temperature and hydrogen peroxide (30%, 2 mL) was added. The next processes, namely, filtration through qualitative filter paper (GEB Co.), washing of remaining solid materials in succession with pure water (200 mL) and hydrochloric acid (10%, 200 mL), centrifugation (6000 rpm for 4 h) of the filtrate by a centrifuge (TG-16-WS XiangYi centrifuge Instruments Co.) and decantation of the supernatant, were

performed. The as-synthesized GO was vacuum-dried overnight at room temperature to yield the desired product.

Preparation of $RGO_{OP-7/EGM}$ sheets

For the reduction process, dry GO (500 mg) was dispersed in a ratio of 3 : 7 of OP-7/EGM (60 : 140 mL) to obtain a solution with high uniformity and good dispersion. The solution was sonicated in a bath-type sonicator (KQ-50, Kunshan Ultrasonic Instruments Co.) for 3 h at a power level of 50 W. Hydrazine hydrate (1 mL) was added, and the mixture was heated at 80 °C for 3 h with constant stirring. The finished product was separated by filtration, washed five times with anhydrous ethanol (400 mL), and vacuum-dried overnight at room temperature to obtain $RGO_{OP-7/EGM}$ powders. Then, 30 mg of the dried $RGO_{OP-7/EGM}$ powder, prepared according to the previous process, was transferred into a tablet mold with an inner diameter of 10 mm and then pressurized (15 MPa) by a hydraulic machine (MLN, QJD2518003). $RGO_{OP-7/EGM}$ sheets can be obtained after holding the pressure for 10 min, followed by demolding.

Preparation of RGO_{H2O} sheets

For the reduction process, dry GO (500 mg) was dispersed in pure water and sonicated for 3 h at a power level of 50 W. Then, $N_2H_4 \cdot H_2O$ (1 mL) was added and the mixture was heated at 80 °C for 3 h with constant stirring. The finished product was separated by filtration and vacuum-dried overnight at room temperature to obtain RGO_{H2O} powders. RGO_{H2O} sheets can be obtained after holding the pressure (15 MPa) for 10 min, followed by demolding.

Characterization of GO, $RGO_{OP-7/EGM}$ and RGO_{H2O} sheets

Fourier transform infrared (FTIR) spectra were recorded on an FTIR spectrometer (Thermo Scientific Nicolet 6700, U.S.) to identify the functional groups. Raman spectra were collected via a confocal microscopic Raman spectrometer (Renishaw InVia Raman microscope, Britain) using a $\times$50 objective lens at room temperature, with a 530 nm laser beam and 1800 lines per mm grating. The UV-vis absorption spectra were recorded by a UV-vis spectrometer (Lambda 750 S, U.S.). Measurement of the interlayer distance of the GOs and RGOs was conducted on XRD (D8 Focus 3 KW, Bruker AXS, Germany) with Cu-Kα radiation (λ = 1.5406 Å). Elemental composition analyses were performed via X-ray photoelectron spectroscopy (XPS, ESCALAB 250Xi) with a monochromatic Al-Kα X-ray source at 100 W. The scanned energy has pass energies of 140.00 eV, and the high-resolution scans have a flux of 26.00 eV. The microstructure and crystal structure were observed by field emission transmission electron microscopy (FETEM, JEM-2100F, Japan) and field emission scanning electron microscopy (FESEM, Zeiss Ultra Plus, Germany). Furthermore, selected area electron diffraction (SAED) was performed using FETEM. Sheet resistance (R_s, Ω sq^{-1}) of the RGO sheets was measured by a four-point probe method (RTS-8, China), and the corresponding volume conductivity (σ, S m^{-1}) can be converted using the formula: $\sigma = 1/(R_s \times t)$, where t indicates the thickness of the RGO sheet.
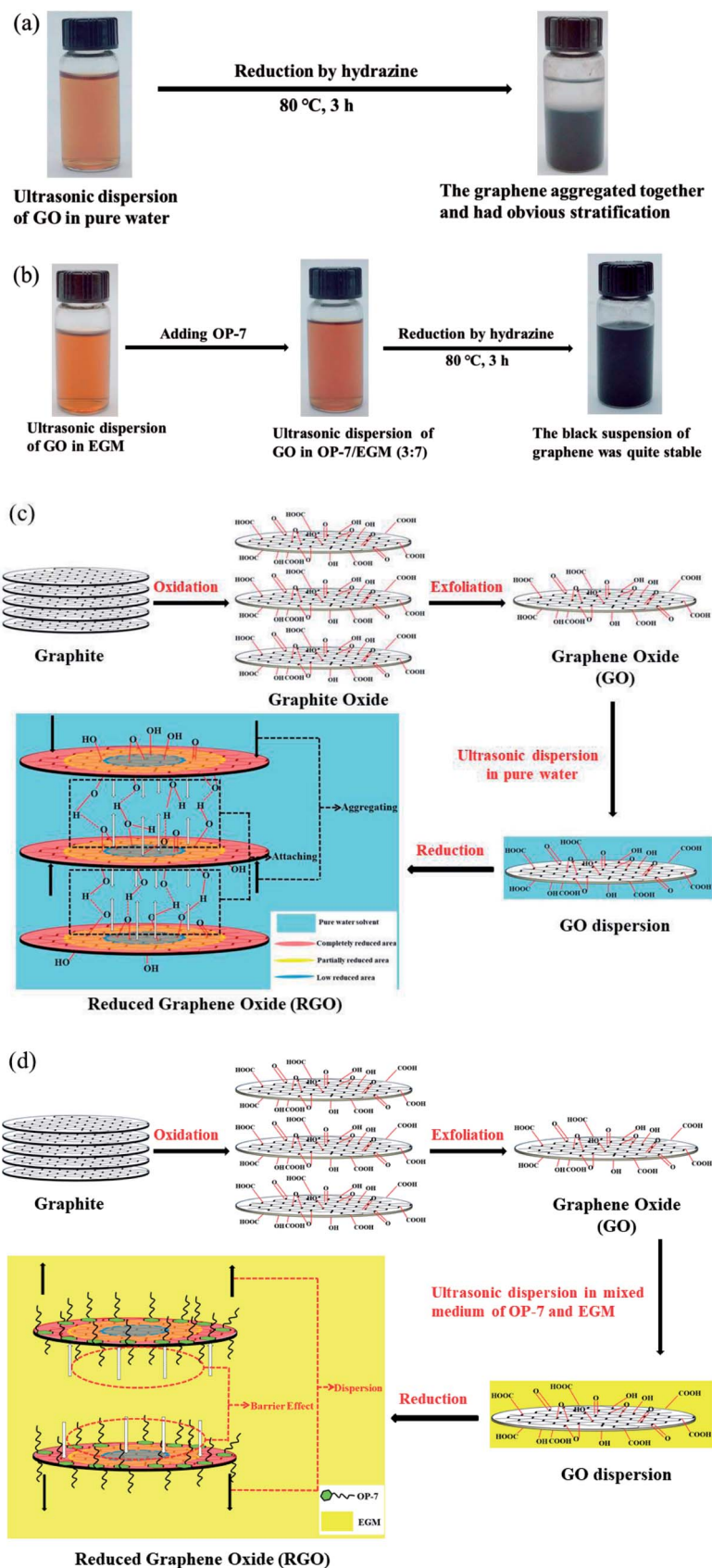
Fig. 1   Reduction routes of GO in pure water (a) and in the mixed reaction medium (OP-7 and EGM) (b); the cause of aggregation in pure water (c) and the aggregation prevention mechanism in the mixed reaction medium (OP-7 and EGM) (d).
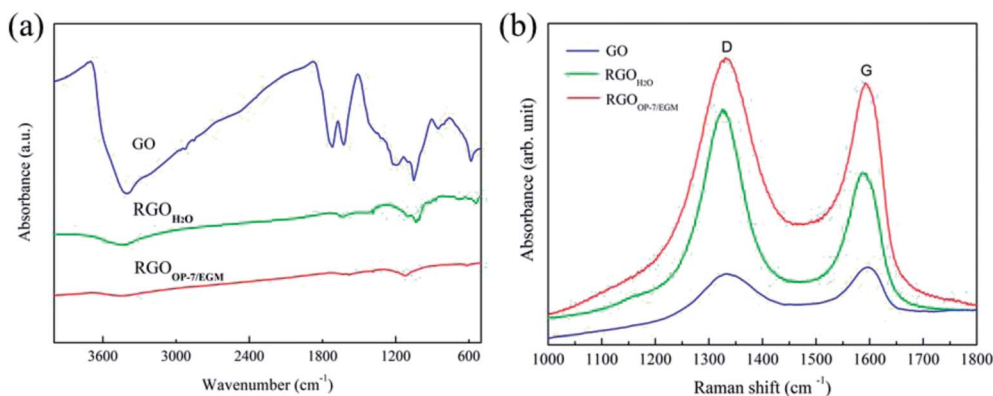
Fig. 2 Fourier transform infrared spectra of GO, RGO$_{H2O}$ and RGO$_{OP-7/EGM}$ (a) and Raman spectra of GO, RGO$_{H2O}$ and RGO$_{OP-7/EGM}$ (b).

Results and discussion

Pure water has been used by many groups as a reaction medium to reduce the GO. However, several chemical reduction reactions in pure water cannot bring about effective excellent performance of the resultant GO. The underlying correlation with reaction medium has not been clearly observed. For this purpose, we compared graphene obtained by reduction in pure water and that in OP-7/EGM mixed medium. Fig. 2a shows the Fourier transform infrared spectra, confirming the different functional groups between GO, RGO$_{H2O}$ and RGO$_{OP-7/EGM}$. The spectrum of GO shows too many peaks: wide and strong O–H stretching vibrations (3410 cm^{-1}), C=O stretching vibrations (1724 cm^{-1}), C=C from sp^2 bonds (1628 cm^{-1}), C–OH stretching vibrations (1220 cm^{-1}), C–O–C stretching vibrations (1050 cm^{-1}) in epoxy, and epoxy stretching vibrations (853 cm^{-1}). The C=O, C–OH and epoxy stretching vibrations evidently disappeared, indicating that the GO has been reduced. On comparing the spectrum of RGO$_{OP-7/EGM}$ with that of RGO$_{H2O}$, we see that O–H and C–O–C stretching vibrations were hardly visible. This indicated that most of the oxygen groups on GO have been removed. This result shows that the edge and center of GO reduced completely under OP-7/EGM mixed reaction medium.

The information of the defects was reflected in the ratio of the intensities of D and G bands (D : G) in the micro-Raman spectra, as shown in Fig. 2b. The G band reflects the symmetry and crystallinity of the material, while the D band is often called the defect band. It can be seen that the intensity ratio (I_D/I_G) of D band and G band of GO is lower than the I_D/I_G of RGO$_{H2O}$ and RGO$_{OP-7/EGM}$. This is due to the presence of

unpaired defects that remained after the removal of a large number of oxygen-containing functional groups.[39] Moreover, the I_D/I_G of RGO$_{H2O}$ increased more significantly than RGO$_{OP-7/EGM}$, indicating that RGO$_{OP-7/EGM}$ has fewer defects after reduction in the mixed reaction medium. This finding shows that OP-7 plays a crucial barrier role in preventing aggregation, which is consistent with previous infrared spectra results. Table 1 lists the physical values of the Raman spectra.

The restoration of C=C bonds during reduction was characterized by UV-vis spectrometry. As shown in Fig. 3, GO has a strong absorption peak at 235 nm and a distinct shoulder at 300 nm. The absorption peak of GO at around 235 nm gradually red-shifted towards 268 nm after reduction of GO. Furthermore, the absorbance in the whole spectral region increased, indicating that the C=C bonds have been restored. The absorption peak shifted to 275 nm, and the absorption was saturated after reducing in mixed medium, indicating that the reduction had been completed.

The powder XRD patterns of graphite (G) and GO were compared with those of the as-prepared RGOs, as shown in Fig. 4a. RGO$_{OP-7}$ and RGO$_{EGM}$ were prepared by reducing GO in pure OP-7 and the pure solution of EGM, respectively; the
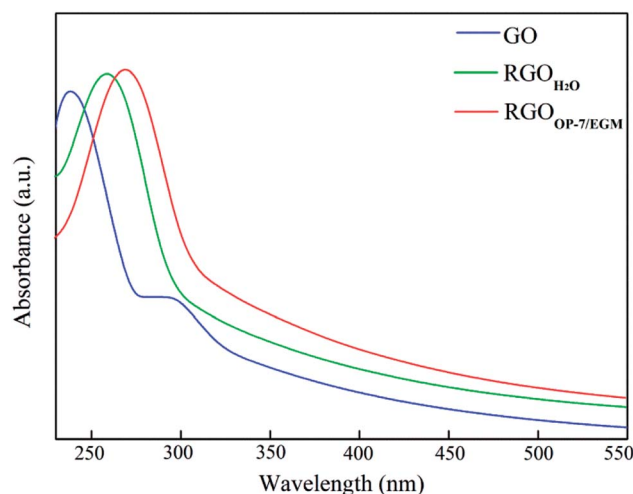
Table 1 Raman spectroscopy of G, GO, RGO$_{H2O}$ and RGO$_{OP-7/EGM}$

	Raman		
	D band (cm^{-1})	G band (cm^{-1})	I_D/I_G (%)
Graphite	—	—	—
GO	1357	1597	0.97
RGO$_{H2O}$	1332	1587	1.37
RGO$_{OP-7/EGM}$	1354	1591	1.01

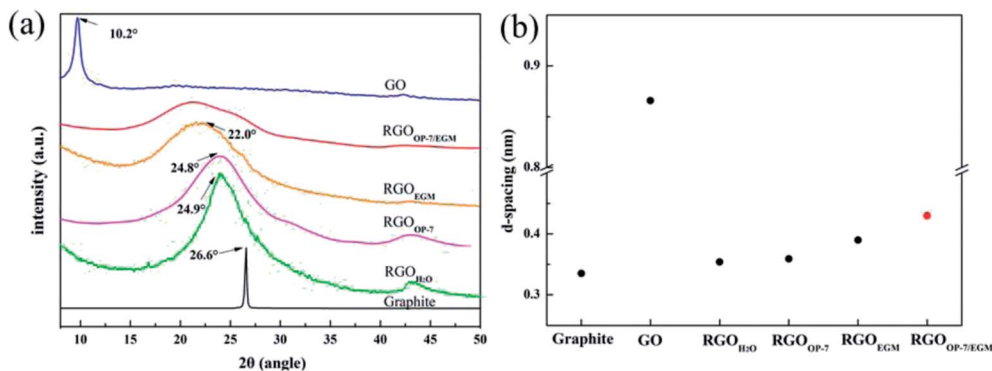Fig. 3 UV-vis absorption spectra of GO, RGO$_{H2O}$ and RGO$_{OP-7/EGM}$.

Fig. 4 XRD patterns of GO, Graphite (G) and RGOs (a) and *d*-spacing for the indicated sample types (b).

preparation routes of RGO_{OP-7} and RGO_{EGM} are shown in Fig. S1.† The peak position for G was $2\theta = 26.60°$ (*d*-spacing $\sim$ 3.35 Å). After the oxidation reaction, GO exhibited a large interlayer distance (*d*-spacing $= \sim 8.66$ Å, $2\theta = 10.20°$) because of the information of hydroxyl, carboxyl and epoxy groups. There was a significant decrease in the average interlayer distance of RGOs after reduction reaction, as described in Fig. 4b. Furthermore, Fig. 4a shows that RGO_{H2O} has a distinct sharp peak, and its interlayer distance decreases to 3.54 Å ($2\theta = 24.92°$), indicating that the RGO_{H2O} has an ordered layer structure because of aggregation during the reduction phase. Although OP-7 can effectively prevent the aggregation of graphene, GO tends to agglomerate in a high concentration of OP-7, resulting in a low reduction degree of GO. The XRD spectrum of RGO_{OP-7} also displays an evident peak at $2\theta = 24.80°$ (*d*-spacing $= \sim 3.59$ Å), which is similar to the peak position of RGO_{H2O}, indicating that RGO_{OP-7} still has a certain layer structure. In addition, the XRD spectrum of RGO_{EGM} has no visible sharp peak, but an inconspicuous broad peak. The interlayer distance of RGO_{EGM} was 3.94 Å ($2\theta = 22.55°$), which was higher than that of RGO_{OP-7} because the solution of EGM can effectively disperse GO. However, the layered structure still exists in RGO_{EGM} because the dispersion of graphene in EGM was not so ideal. If we only simply satisfy the good dispersion of GO or prevent graphene aggregation, it will be difficult to prepare graphene with good properties. Based on a comparison with interlayer spacing of graphene previously prepared by chemical reduction methods, we found that the spacing of the graphene layers was between 3.57 Å and 3.90 Å, while they all had a distinct sharp diffraction peak.[27–30,36] On the contrary, a dispersing and broad diffraction peak between 22.0° and 26.9° can be observed in the XRD pattern of $RGO_{OP-7/EGM}$. This shows that $RGO_{OP-7/EGM}$ has no typical layered structure because of the barrier effect of OP-7 and the good dispersion action of EGM. As shown in Fig. S2,† we calculated that the distance between the donor hydrogen and the acceptor oxygen atoms bonded to different functional groups of two graphene sheets was between 3.63 Å and 4.05 Å. This calculated result was consistent with the layer spacing of graphene prepared by the previous chemical methods and indicated that the individual graphene layers fit with each other *via* hydrogen bonds mediated by oxygen-containing functional groups. The average interlayer distance

of $RGO_{OP-7/EGM}$ was 4.21 Å, corresponding to the red dot in Fig. 4b, which was higher than 4.05 Å owing to the prevention of the formation of hydrogen bonds by OP-7. In general, the barrier effect of OP-7 and the dispersion effect of EGM are indispensable in the preparation of graphene.

The C/O ratio and information about various functional groups of GO, RGO_{H2O} and $RGO_{OP-7/EGM}$ were investigated by X-ray photoemission spectroscopy (XPS). In Fig. 5a, the O 1s peak and C 1s peak positions are observed at 284.8 eV and 533.0 eV, respectively. Through the comparison of GO and RGO_{H2O}, we found that the intensity of the O 1s peak of RGO_{H2O} visibly decreased in the broad region. This implied that the C/O ratio of RGO increased significantly after reduction due to the removal of oxygen-containing groups. In addition, the intensity of the O 1s peak of $RGO_{OP-7/EGM}$ was slightly lower than that of RGO, suggesting that $RGO_{OP-7/EGM}$ was reduced more completely. Fig. 5b shows the C 1s spectrum of GO, which reveals that it consists of two main components arising from the C=C/C–C (284.6 eV) and C=O (carbonyl, $\sim$288.3 eV) groups and two minor components from the C–O (hydroxyl and epoxy, $\sim$286.5 eV) and O–C=O (carboxyl, $\sim$290.3 eV) groups.[40] After reduction by the traditional chemical method, the C 1s XPS spectrum of RGO_{H2O} also displayed these peaks, but their intensities were much lower than those of GO (Fig. 5c), indicating that most of the oxygen functional groups were removed. Most of the C=O bonds (carbonyl groups, $\sim$286.9 eV) were converted into C–O bonds (hydroxyl groups, $\sim$286.1 eV), and a number of carboxyl groups were removed. By using mixed reaction medium of OP-7 and EGM, all of the carbonyl groups of $RGO_{OP-7/EGM}$ were almost completely removed, and the C–O bonds were reduced, as shown in Fig. 5d. Compared with RGO_{H2O}, the reduction degree of $RGO_{OP-7/EGM}$ is higher. Areas of the contributing peaks are listed in Table 2. The atomic ratio of C/O increased from 1.70 for GO to 9.04 for $RGO_{OP-7/EGM}$, which was higher than the value for the RGO_{H2O} obtained by reduction in pure water. The C–C groups of $RGO_{OP-7/EGM}$ compared with RGO_{H2O} increased substantially, while the C–O and C=O groups decreased significantly and the O–C=O groups disappeared completely. These results show that $RGO_{OP-7/EGM}$ was reduced much better than RGO_{H2O}, which is consistent with the XRD spectra due to the barrier effect of surfactant OP-7 and the great dispersion action of EGM.
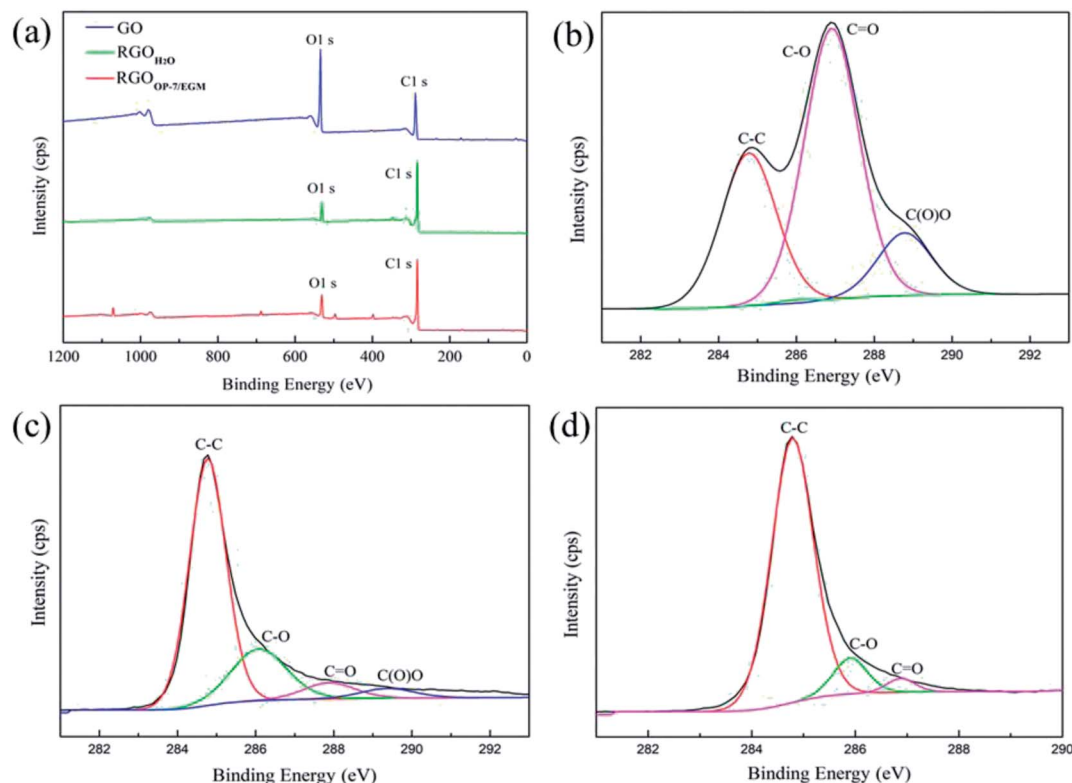
Fig. 5 XPS spectra of GO, RGO$_{H2O}$ and RGO$_{OP-7/EGM}$: wide region (a) and C 1s region of GO (b), RGO$_{H2O}$ (c) and RGO$_{OP-7/EGM}$ (d).

As shown in Fig. 6a, a field emission scanning electron microscopy (FESEM) image of the surface of the RGO$_{H2O}$ power sample exhibited many stacks due to aggregation. On the contrary, a clearly single-layer structure of the RGO$_{OP-7/EGM}$ sheet is observed in Fig. 6b. Fig. 6c shows the field emission transmission electron microscopy (FETEM) image of the RGO$_{H2O}$ sheets; we can find that the RGO$_{H2O}$ sheets overlapped and aggregated into a multilayer structure. Fig. 6d and e show the TEM images of the RGO$_{OP-7/EGM}$ platelets at different magnifications, respectively. Although a few folds appear on the RGO$_{OP-7/EGM}$ sheets, most of the graphene sheets were single-layer or few-layer owing to the complementary role of OP-7 and EGM. As can be seen in Fig. 6f, the selected area electron diffraction (SAED) pattern distinctly indicates the graphitic crystalline structure. The first ring came from the (1100) plane, and the bright spots consistent with the (1100) reflections retained the hexagonal symmetry of the [0001] diffraction pattern. Furthermore, we found that the relative strength of the inner and outer spot rings was close,

corresponding to the structure of single-layer graphene or few layer graphene.

Table 3 summarizes the electrical conductivity of RGO$_{H2O}$, RGO$_{OP-7}$, RGO$_{EGM}$ and RGO$_{OP-7/EGM}$ sheets dried at room temperature. The conductivity of RGO$_{H2O}$ was only 1050 S m^{-1} because hydrophobic graphene sheets were easily aggregating in an aqueous environment. The conductivity of RGO$_{OP-7}$ was 1400 S m^{-1}, which was similar to that of RGO$_{H2O}$, because GO tended to aggregate in a high concentration of OP-7, resulting in a low reduction degree of GO. Although the conductivity of RGO$_{EGM}$ increased to 3770 S m^{-1}, the poor dispersion of graphene in EGM led to non-ideal conductivity. With the use of the mixed reaction medium of OP-7 and EGM, the conductivity of RGO$_{OP-7/EGM}$ was 14 000 S m^{-1}, showing an over tenfold increase with respect to the RGO$_{H2O}$ value due to the interactions between the barrier effect of OP-7 and the good dispersion action of EGM. This result is consistent with the previous test results.

Table 2 The C 1s peak position and the relative atomic percentage of various functional groups in GO, RGO$_{H2O}$ and RGO$_{OP-7/EGM}$

	Fitting of the C 1s peak binding energy [eV] (relative atomic percentage [%])				XPS
	C–C	C–O/C–O–C	C=O	O–C=O	C : O ratio
GO	284.78 (31.55)	286.01 (1.48)	286.91 (55.33)	288.78 (11.64)	1.70
RGO$_{H2O}$	284.77 (67.98)	286.08 (21.74)	287.88 (6.30)	289.38 (3.98)	6.25
RGO$_{OP-7/EGM}$	284.79 (89.33)	285.90 (8.62)	286.88 (2.05)	—	9.04
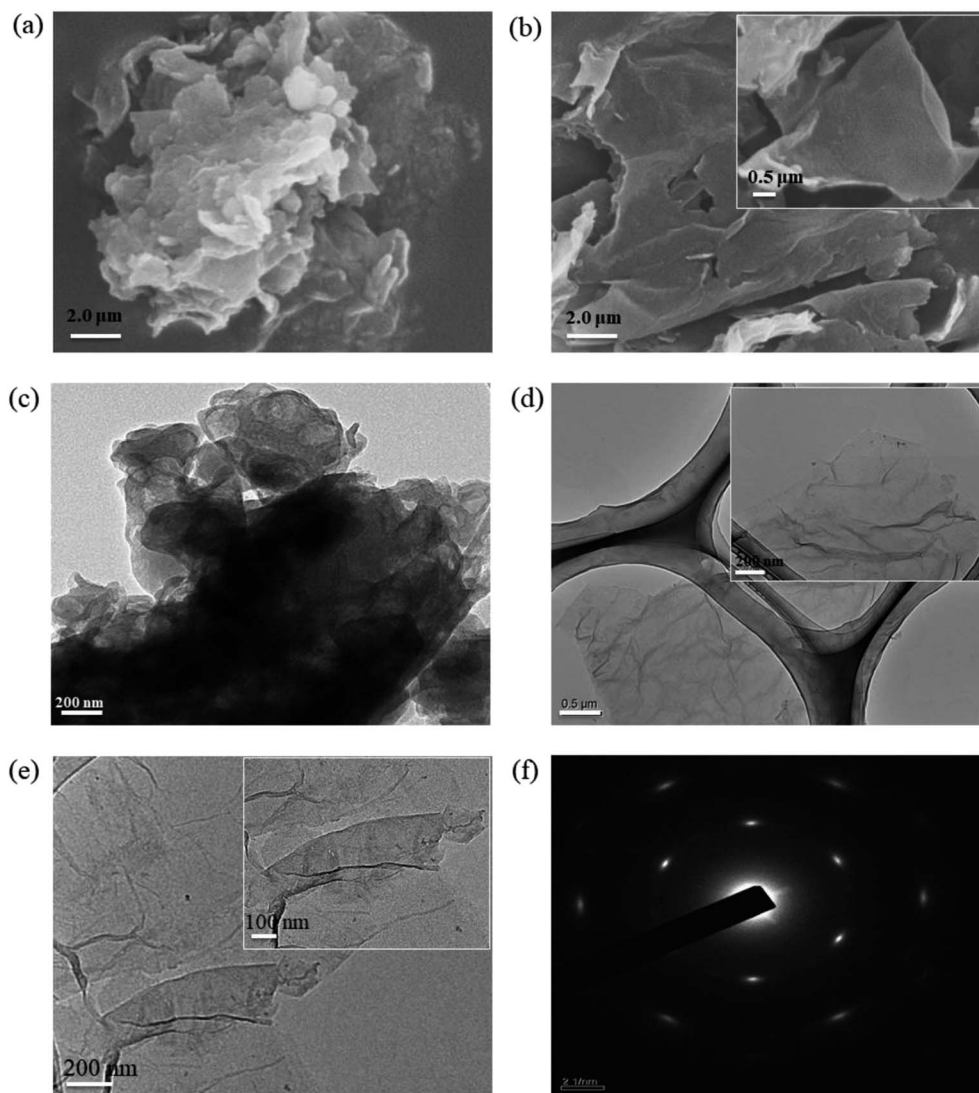
Fig. 6 SEM images of RGO$_{H2O}$ (a) and RGO$_{OP-7/EGM}$ (b), TEM image of RGO$_{H2O}$ (c), TEM images of RGO$_{OP-7/EGM}$ (d) and (e) at different magnifications, SAED pattern of RGO$_{OP-7/EGM}$ platelet (f).

Table 3 Electrical conductivities of RGO$_{H2O}$, RGO$_{OP-7}$, RGO$_{EGM}$ and RGO$_{OP-7/EGM}$ sheets

Reduced graphene oxide	Drying temperature	Conductivity (S m^{-1})
RGO$_{H2O}$	Room temperature	1050
RGO$_{OP-7}$	Room temperature	1400
RGO$_{EGM}$	Room temperature	3770
RGO$_{OP-7/EGM}$	Room temperature	14 000

Table 4 summarizes the electrical conductivity of the RGO$_{OP-7/EGM}$ power pellets and graphene power pellets or free-standing paper samples under different reduction conditions. In contrast to the electrical conductivity reported previously for modified graphene reduced by different chemical methods, our RGO$_{OP-7/EGM}$ power pellet had a high electrical conductivity (14 000 S m^{-1}), which was almost 70 times that of graphene reduced by hydrazine (200 S m^{-1}), and achieved a higher value without treatment at high-temperatures. The conductivity of RGO$_{HI-AcOH}$ reduced by hydroiodic acid (HI) in acetic acid (AcOH) solvent is higher than that of RGO$_{OP-7/EGM}$, the final conductivity of graphene may be different due to the differences in the reduction system. Our method of reduction in the mixed medium of OP-7 and EGM is a simple separation process, involves mild reaction conditions and short reduction time, and exhibits great reproducibility. The high electrical conductivity of RGO$_{OP-7/EGM}$ was attributed to the avoidance of aggregation because of the barrier effect of surfactant OP-7 and the good dispersion action of the organic solvent EGM. The electrical conductivity of RGO$_{OP-7/EGM}$ with 220 °C treatment reached 15 800 S m^{-1}, which was higher than that of the RGO$_{OP-7/EGM}$ sheet (14 000 S m^{-1}) obtained via room temperature treatment. We consider that the increase in electrical conductivity could be attributed to the escape and volatilization of some organic matter or adsorbate on the surface of RGO$_{OP-7/EGM}$.

Table 4 Electrical conductivities of the RGO power pellet and free-standing paper samples of modified graphene

Reduced graphene oxide	Reduction temperature (°C)	Reduction time (h)	Drying temperature (°C)	Conductivity (S m^{-1})
RGO$_{OP-7/EGM}$	80	3	Room temperature	14 000
			220	15 800
Reduced graphene oxide by hydrazine[33]	80	24	60	200
RGO$_{HI-AcOH}$[28]	40	40	Room temperature	30 400
hKMG[34]	35	6	Room temperature	690
RGH[35]	90	48	−37 °C freeze-dried	1351
HRG[36]	80	12	Room temperature	1700
			150	16 000
CCG[31,32]	95	1	Room temperature	7200
			220	11 800
CCG2 (ref. 25)	120	12	Room temperature	1600

Conclusions

In summary, we have analyzed the aggregation of graphene during the chemical reduction method and reported the method to prevent the aggregation of graphene. In addition, the potential reduction mechanism and the root cause for the aggregation of graphene have been addressed. RGO$_{OP-7/EGM}$ was reduced from GO with hydrazine hydrate in a mixed medium of OP-7 and EGM. EGM provided a good dispersion environment for GO, and OP-7 could effectively prevent superimposed aggregation. Furthermore, the XRD spectrum of RGO$_{OP-7/EGM}$ shows a dispersing diffraction peak, indicating that there was no typical layer structure. The RGO$_{OP-7/EGM}$ sheet obtained *via* room temperature treatment had an electrical conductivity value as high as 14 000 S m^{-1}.

Conflicts of interest

We declare that we have no financial and personal relationships with other people or organizations that can inappropriately influence our work. There is no professional or other personal interest of any nature or kind in any product, service and/or company that could be construed as influencing the position presented in, or the review of, the manuscript entitled, "Aggregation Prevention: Reduction of Graphene Oxide in Mixed Medium of Alkylphenol Polyoxyethylene (7) Ether and 2-Methoxyethanol".

Acknowledgements

References

1 A. K. Geim, *Science*, 2009, **324**, 1530–1534.
2 A. K. Geim and K. S. Novoselov, *Nat. Mater.*, 2007, **6**, 183–191.
3 S. Ramirez, K. Chan, R. Hernandez, E. Recinos, E. Hernandez, R. Salgado, A. G. Khitun, J. E. Garay and A. A. Balandin, *Mater. Des.*, 2017, **118**, 75–80.
4 X. Wang, L. Zhi and K. Müllen, *Nano Lett.*, 2008, **8**, 323–327.
5 R. Verma, S. Bhattacharya and S. Mahapatra, *IEEE Trans. Electron Devices*, 2013, **60**, 2695–2698.
6 C. N. R. Rao, A. K. Sood, K. S. Subrahmanyam and A. Govindaraj, *Angew. Chem., Int. Ed.*, 2009, **48**, 52–77.
7 H. Bai, C. Li and G. Shi, *Adv. Mater.*, 2011, **23**, 1089–1115.
8 B. Guo, L. Fang, B. Zhang and J. R. Gong, *Insci. J.*, 2011, **40**, 80–89.
9 H. Spanggaard and F. C. Krebs, *Sol. Energy Mater. Sol. Cells*, 2004, **83**, 125–146.
10 G. Wang, X. Shen, J. Yao and J. Park, *Carbon*, 2009, **47**, 2049–2053.
11 W. Bower, W. Head, G. T. R. Droop, R. Zan, R. A. D. Pattrick, P. Wincott and S. J. Haigh, *Mineral. Mag.*, 2015, **79**, 337–344.
12 K. Kim, J. Park, C. Kim, W. Choi, Y. Seo, J. Ahn and I. Park, *Micro Nano Lett.*, 2012, **7**, 1133.
13 J. N. Coleman, M. Lotya, A. O'Neill, S. D. Bergin, P. J. King, U. Khan, K. Young, A. Gaucher, S. De, R. J. Smith, I. V. Shvets, S. K. Arora, G. Stanton, H. Y. Kim, K. Lee, G. T. Kim, G. S. Duesberg, T. Hallam, J. J. Boland, J. J. Wang, J. F. Donegan, J. C. Grunlan, G. Moriarty, A. Shmeliov, R. J. Nicholls, J. M. Perkins, E. M. Grieveson, K. Theuwissen, D. W. McComb, P. D. Nellist and V. Nicolosi, *Science*, 2011, **331**, 568–571.
14 D. Long, W. Li, L. Ling, J. Miyawaki, I. Mochida and S. Yoon, *Langmuir*, 2010, **26**, 16096–16102.
15 S. Pei and H. Cheng, *Carbon*, 2012, **50**, 3210–3228.
16 D. Chen, H. Feng and J. Li, *Chem. Rev.*, 2012, **112**, 6027–6053.
17 S. Pei, J. Zhao, J. Du, W. Ren and H. Cheng, *Carbon*, 2010, **48**, 4466–4474.
18 R. Iguchi, T. Kawamura, Y. Suzuki, M. Inoue, Y. Kangawa and K. Kakimoto, *Jpn. J. Appl. Phys.*, 2014, **53**, 65601.
19 Z. Juang, C. Wu, C. Lo, W. Chen, C. Huang, J. Hwang, F. Chen, K. Leou and C. Tsai, *Carbon*, 2009, **47**, 2026–2031.
20 B. Hu, H. Ago, Y. Ito, K. Kawahara, M. Tsuji, E. Magome, K. Sumitani, N. Mizuta, K. Ikeda and S. Mizuno, *Carbon*, 2012, **50**, 57–65.
21 M. Batzill, *Surf. Sci. Rep.*, 2012, **67**, 83–115.
22 W. S. Hummers Jr and R. E. Offeman, *J. Am. Chem. Soc.*, 1958, **80**, 1339.

23 L. Tang, Y. Wang, Y. Li, H. Feng, J. Lu and J. Li, *Adv. Funct. Mater.*, 2009, **19**, 2782–2789.

24 A. F. Morpurgo, H. B. Heersche, L. M. K. Vandersypen, X. Liu and J. B. Oostinga, *Nat. Mater.*, 2008, **7**, 151–157.

25 W. Gao, L. B. Alemany, L. Ci and P. M. Ajayan, *Nat. Chem.*, 2009, **1**, 403–408.

26 S. Pei, J. Zhao, J. Du, W. Ren and H. Cheng, *Carbon*, 2010, **48**, 4466–4474.

27 H. Shin, K. K. Kim, A. Benayad, S. Yoon, H. K. Park, I. Jung, M. H. Jin, H. Jeong, J. M. Kim, J. Choi and Y. H. Lee, *Adv. Funct. Mater.*, 2009, **19**, 1987–1992.

28 I. K. Moon, J. Lee, R. S. Ruoff and H. Lee, *Nat. Commun.*, 2010, **1**, 1–6.

29 Z. Fan, K. Wang, T. Wei, J. Yan, L. Song and B. Shao, *Carbon*, 2010, **48**, 1686–1689.

30 V. H. Pham, T. V. Cuong, T. D. Nguyen-Phan, H. D. Pham, E. J. Kim, S. H. Hur, E. W. Shin, S. Kim and J. S. Chung, *Chem. Commun.*, 2010, **46**, 4375–4377.

31 D. Li, M. B. Mã Ller, S. Gilje, R. B. Kaner and G. G. Wallace, *Nat. Nanotechnol.*, 2008, **3**, 101–105.

32 H. Chen, M. B. Müller, K. J. Gilmore, G. G. Wallace and D. Li, *Adv. Mater.*, 2008, **20**, 3557–3561.

33 C. Bao, L. Song, W. Xing, B. Yuan, C. A. Wilkie, J. Huang, Y. Guo and Y. Hu, *J. Mater. Chem.*, 2012, **22**, 688–696.

34 S. Park, J. An, R. D. Piner, I. Jung, D. Yang, A. Velamakanni, S. T. Nguyen and R. S. Ruoff, *Chem. Mater.*, 2008, **20**, 6592–6594.

35 V. H. Luan, H. N. Tien, L. T. Hoa, N. T. M. Hien, E. Oh, J. Chung, E. J. Kim, W. M. Choi, B. Kong and S. H. Hur, *J. Mater. Chem. A*, 2013, **1**, 208–211.

36 S. Park, J. An, I. Jung, R. D. Piner, S. J. An, X. Li, A. Velamakanni and R. S. Ruoff, *Nano Lett.*, 2009, **9**, 1593–1597.

37 D. Chen, H. Feng and J. Li, *Chem. Rev.*, 2012, **112**, 6027–6053.

38 X. Gao, J. Jang and S. Nagase, *J. Phys. Chem. C*, 2009, **114**, 832–842.

39 Y. Zhou, Q. Bao, L. A. L. Tang, Y. Zhong and K. P. Loh, *Chem. Mater.*, 2009, **21**, 2950–2956.

40 S. Stankovich, D. A. Dikin, R. D. Piner, K. A. Kohlhaas, A. Kleinhammes, Y. Jia, Y. Wu, S. T. Nguyen and R. S. Ruoff, *Carbon*, 2007, **45**, 1558–1565.